

Spectroscopic and Kinetic Studies of the Reaction of Bromopropanesulfonate with Methyl-coenzyme M Reductase^{*[5]}

Received for publication, July 14, 2006, and in revised form, August 29, 2006. Published, JBC Papers in Press, September 11, 2006, DOI 10.1074/jbc.M606715200

Ryan C. Kunz, Yih-Chern Horng¹, and Stephen W. Ragsdale²

From the Department of Biochemistry, University of Nebraska, Lincoln, Nebraska 68588-0664

Methyl-coenzyme M reductase (MCR) catalyzes the final step of methanogenesis in which coenzyme B and methyl-coenzyme M are converted to methane and the heterodisulfide, CoMS-SCoB. MCR also appears to initiate anaerobic methane oxidation (reverse methanogenesis). At the active site of MCR is coenzyme F₄₃₀, a nickel tetrapyrrole. This paper describes the reaction of the active MCR_{red1} state with the potent inhibitor, 3-bromopropanesulfonate (BPS; I₅₀ = 50 nM) by UV-visible and EPR spectroscopy and by steady-state and rapid kinetics. BPS was shown to be an alternative substrate of MCR in an ionic reaction that is coenzyme B-independent and leads to debromination of BPS and formation of a distinct state ("MCR_{PS}") with an EPR signal that was assigned to a Ni(III)-propylsulfonate species (Hinderberger, D., Piskorski, R. P., Goenrich, M., Thauer, R. K., Schweiger, A., Harmer, J., and Jaun, B. (2006) *Angew. Chem. Int. Ed. Engl.* 45, 3602–3607). A similar EPR signal was generated by reacting MCR_{red1} with several halogenated sulfonate and carboxylate substrates. In rapid chemical quench experiments, the propylsulfonate ligand was identified by NMR spectroscopy and high performance liquid chromatography as propanesulfonic acid after protonolysis of the MCR_{PS} complex. Propanesulfonate formation was also observed in steady-state reactions in the presence of Ti(III) citrate. Reaction of the alkyl-nickel intermediate with thiols regenerates the active MCR_{red1} state and eliminates the propylsulfonate group, presumably as the thioether. MCR_{PS} is catalytically competent in both the generation of propanesulfonate and reformation of MCR_{red1}. These results provide evidence for the intermediacy of an alkylnickel species in the final step in anaerobic methane oxidation and in the initial step of methanogenesis.

Methanogens are strictly anaerobic microbes in the kingdom Archaea that form methane to generate cellular energy. Approximately 1 billion tons of methane are produced by these anaerobic microorganisms per year (1), which generates signif-

icant amounts of a valuable fuel but poses a potential environmental problem because methane is a potent greenhouse gas. Methyl-coenzyme M reductase (MCR)³ catalyzes the final step in biological methane formation: the reaction of methyl-coenzyme M (methyl-SCoM) with *N*-7-mercaptoheptanoyl-threonine phosphate (HSCoB) to generate methane and the mixed disulfide CoBS-SCoM (Reaction 1) (1, 2). HSCoB serves as the two-electron donor (3). At the active site of MCR is a nickel tetrapyrrolic cofactor called coenzyme F₄₃₀ that is central to catalysis (4–6). X-ray crystallographic studies reveal that coenzyme F₄₃₀ binds noncovalently to MCR at the bottom of a 30-Å hydrophobic channel (7). The phosphate group of HSCoB binds at the upper lip of this channel with its thiol group located 8.7 Å from the central nickel atom of F₄₃₀.



$$\Delta G = -30 \text{ kJ/mol} \quad (\text{Eq. 1})$$

MCR can exist in several states that differ in their nickel oxidation and/or coordination states (Fig. 1). The MCR_{red1} state is catalytically active (8–10) based on the correlation between the amount of this enzyme form and MCR activity in *Methanothermobacter marburgensis* (10) and *Methanosarcina thermophila* (11). MCR_{ox1} appears to be the only state that can be converted *in vitro* to active MCR_{red1}, which is accomplished by incubating the MCR_{ox1} state with a strong reductant, titanium(III) citrate (Ti(III) citrate) (10). The MCR_{red1} state also can be generated *in vivo* when cells are bubbled with 100% H₂ before harvesting (8). MCR_{ox1} can be formed when the gas medium of growing cells is switched before harvesting from 80% H₂, 20% CO₂ to 80% N₂, 20% CO₂ (8) or by treating the growing cells with sodium sulfide (11).

High resolution crystal structures for three EPR-silent and inactive Ni(II) states of this enzyme have been determined: MCR_{silent}, MCR_{ox1-silent}, and MCR_{red1-silent} (7, 12, 13). These states have several common features: the central nickel atom of

^{*} This work was supported by Department of Energy Grant DE-FG03-ER20297 and Center Grant 1P20RR17675 (to the University of Nebraska). The costs of publication of this article were defrayed in part by the payment of page charges. This article must therefore be hereby marked "advertisement" in accordance with 18 U.S.C. Section 1734 solely to indicate this fact.

[5] The on-line version of this article (available at <http://www.jbc.org>) contains supplemental Figs. S1 and S2.

¹ Present address: Dept. of Chemistry, National Changhua University of Education, Changhua 50058, Taiwan.

² To whom correspondence should be addressed. Tel.: 402-472-2943; Fax: 402-472-7842; E-mail: sragsdale1@unl.edu.

³ The abbreviations used are: MCR, methyl-coenzyme M reductase; BPS, bromopropanesulfonate; HSCoB, coenzyme B; methyl-SCoM, methyl-coenzyme M; HSCoM, coenzyme M; HPLC, high performance liquid chromatography; BPS, 3-bromopropanesulfonate; DFT, density functional theory; PS, propylsulfonate; HPS, propanesulfonate; TAPS, 3-[(2-hydroxy-1,1-bis(hydroxymethyl)ethyl)amino]-1-propanesulfonic acid; BES, 2-[bis(2-hydroxyethyl)amino]ethanesulfonic acid; MES, 2-(*N*-morpholino)ethanesulfonic acid; CAPS, 3-(cyclohexylamino)propanesulfonate; BBS, 4-bromo-1-butanethanesulfonate; MOPS, 3-(*N*-morpholino)propanesulfonic acid; CHES, 2-(cyclohexylamino)ethanesulfonic acid.

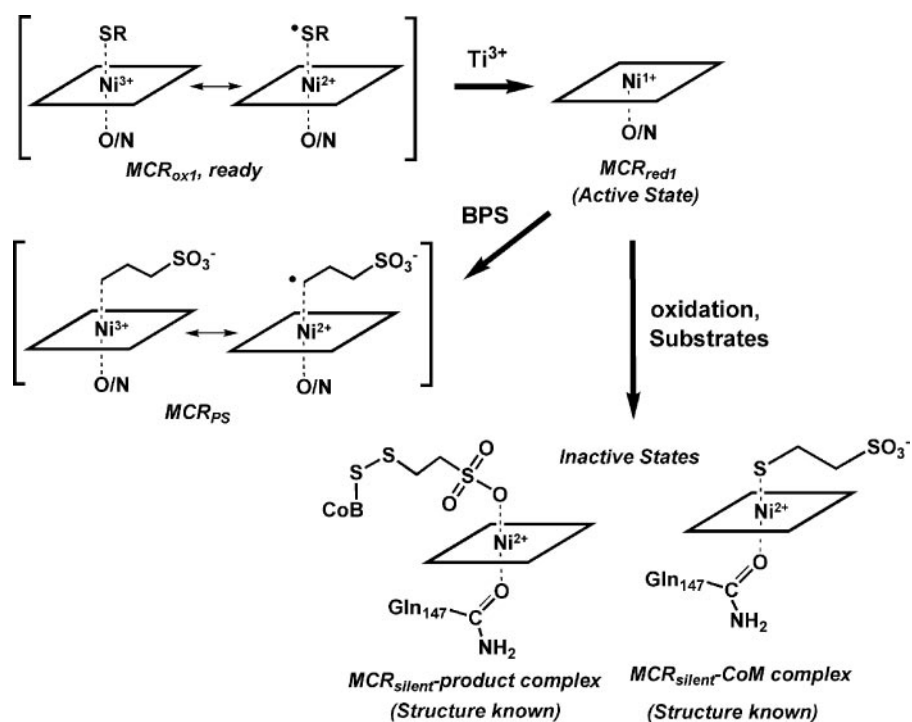


FIGURE 1. Coordination environment of Ni-F₄₃₀ in various states of methyl-coenzyme M reductase. S-CH₂-CH₂-SO₃⁻ is coenzyme M, -SO₃-CH₂-CH₂-S-S-CoB is the heterodisulfide, and H₂N-CO- is glutamine residue Gln-α147. The crystal structures of the MCR_{ox1}, MCR_{ps}, and MCR_{red1} states have not been solved. The oxidation state and coordination environment of nickel in these two states are described in the Introduction.

F₄₃₀ is coordinated by four planar tetrapyrrole nitrogen atoms and a lower axial oxygen ligand contributed by the carbonyl oxygen of the side chain of Gln-α'147. In the Ni(II)_{silent} form of MCR, the upper axial nickel ligand is the sulfonate oxygen of CoBS-SCoM, whereas, in the Ni(II)_{ox1-silent} form, this site is occupied by the thiol(ate) group of CoM-S(H) (Fig. 1) (7, 12, 13). A five-coordinate form of Ni(II)-MCR_{red1-silent}, lacking an upper axial ligand, has also been observed in the crystal structure (13). The structures of "ready" MCR_{ox1} and "active" MCR_{red1} forms have not yet been determined, since they are quite labile. Based on an array of spectroscopic (x-ray absorption (14), UV-visible (15, 16), EPR (14, 17), pulsed EPR (17), and magnetic circular dichroism (15, 16)) and computational methods (15), MCR_{ox1} is best described as a high spin Ni(II) coupled to a thiol-radical (15, 17) (Fig. 1). MCR_{red1} is known to be in the Ni(I) state (9–11). Recent x-ray absorption results (14, 18) indicate that the nickel is six-coordinate in the MCR_{ox1} state, yet there is still some controversy about the MCR_{red1} state, which is either five-coordinate with an open upper axial site (14) or six-coordinate with two axial ligands coordinated through an oxygen atom (18) (Fig. 1). The coordination state of MCR_{red1} needs to be resolved, because having an open upper axial site would poise the Ni(I) for reaction with substrate, whereas an axial ligand would need to be replaced/removed before reaction could occur. Kinetic studies using several small molecules (CHCl₃, CH₂Cl₂, and NO) and substrate analogs (including 3-bromopropanesulfonate (BPS)) support the requirement for ligand exchange (19); however, further studies are important in resolving this mechanistic question.

Two radically different mechanisms have been proposed for the catalytic mechanism of MCR. In Mechanism I, Ni(I)-

MCR_{red1} reacts with the methyl group of methyl-SCoM, forming a methyl-Ni(III) or methyl-Ni(II) intermediate (20–23). Although the corresponding methyl-nickel species has not been observed on the enzyme, methane formation from the reaction of Ni(I)-derivatives of F₄₃₀ and activated methyl donors like methylsulfonium ions has been observed (24), and a methyl-Ni(II) form of the pentamethyl ester of F₄₃₀ has been characterized by NMR methods (25). Furthermore, reacting Ni(I)-octaethylisobacteriochlorin (a structural cousin of F₄₃₀) with various alkyl halides generates alkyl-Ni(III) species that undergo reduction to the alkyl-Ni(II) followed by protonolysis to yield the corresponding alkane (26).⁴

On the basis of a computational study using density function theory (DFT), the proposed methyl-nickel species was considered to not be a feasible intermediate in methane synthesis, and Mechanism II was

proposed as an alternative to Mechanism I (27). The key steps of Mechanism II include nucleophilic attack by Ni(I)-MCR_{red1} on methyl-SCoM to form a nickel-thiolate complex and a methyl radical, which abstracts a hydrogen atom from HSCoB to generate methane (27).

Unfortunately, it has been difficult to distinguish between these mechanisms, mainly because we have so far been unable to observe any spectrally distinct intermediates by rapid kinetics.⁵ Another complication is that MCR_{red1}-catalyzed cleavage of the C–S bond of methyl-SCoM requires the other substrate, HSCoB, even under single turnover conditions (23). In the studies described here, we used BPS as a substrate analog, because, unlike methyl-SCoM, reduction of BPS in a single turnover reaction does not require the other substrate HSCoB; furthermore, EPR and UV-visible changes can be observed. When MCR_{red1} and MCR_{red2} are incubated with BPS, their EPR signals convert to the MCR_{ps} signal, which does not exhibit measurable halogen-Ni(I) interaction (28) and has been assigned to a high spin Ni(II)/alkyl radical species (29). Here we show that this EPR spectroscopic change is accompanied by formation of an "MCR_{ox1}-like" UV-visible spectrum and the reduction of BPS to propanesulfonate.

EXPERIMENTAL PROCEDURES

Materials and Organisms—*M. marburgensis* (f. *M. thermoautotrophicum* strain Marburg) was obtained from the Oregon

⁴ In these reactions, a stoichiometry of 2 Ni(I)/alkyl halide was observed, indicating reduction of the alkyl-Ni(III) to the alkyl-Ni(II) state before protonolysis.

⁵ Y.-C. Horng and S. W. Ragsdale, unpublished observations.

Collection of Methanogens catalogue as OCM82. All buffers, media ingredients, and other reagents were acquired from Sigma and, unless otherwise stated, were of the highest purity available. Solutions were prepared using Nanopure deionized water. N₂ (99.98%), H₂S (99.0%), CO (99.99%), argon (99.8%), H₂/CO₂ (80%/20%), and ultrahigh purity H₂ (99.999%) were obtained from Linweld (Lincoln, NE).

Methyl-SCoM was prepared from coenzyme M and methyl iodide (30). After methyl-SCoM was crystallized twice in acetone, its purity was checked by ¹H NMR spectroscopy. CoBS-SCoB was prepared as described from 7-bromoheptanoic acid (Karl Industries, Aurora, OH), *N*-hydroxysuccinamide, and *o*-phospho-L-threonine (31, 32). HSCoB was generated from CoBS-SCoB by anaerobic reduction with NaBH₄ (33), and its purity was ascertained by HPLC. The concentration of HSCoB was checked routinely with Ellman's reagent (34) before using it. Ti(III) citrate solutions were prepared from a stock solution of 200 mM Ti(III) citrate, which was synthesized by adding sodium citrate to Ti(III) trichloride (30 weight % solution in 2 N hydrochloric acid) (Acros Organics, Morris Plains, NJ) under anaerobic conditions and adjusting the pH to 7.0 with sodium bicarbonate (35). The concentration of Ti(III) citrate was determined routinely by titrating a methyl viologen solution.

M. marburgensis Growth, Harvest, and Purification Conditions—*M. marburgensis* was cultured on H₂/CO₂/H₂S (80%/20%/0.1%) at 65 °C in a 14-liter fermentor (New Brunswick Scientific Co., Inc., New Brunswick, NJ) (10, 36). Culture media were prepared as previously described (36). Once the culture had reached late log phase (*A*₅₇₈ ~ 3.0), sodium sulfide was added directly to the growing cells (final sulfide concentration, 20 mM) prior to harvesting as described (11). After 15 min at 65 °C, the culture was cooled to 25 °C within 30 min and harvested anaerobically.

MCR_{red1} used in Figs. 2, 5, 8, 9, S1, and S2 was isolated (details below) from *M. marburgensis* cultured on H₂/CO₂/H₂S (80%/20%/0.1%) at 65 °C in a 14-liter fermentor (New Brunswick Scientific) (10, 36). Culture media were prepared as previously described (36). MCR_{red1} was generated *in vivo* as described with the following modifications (8, 37). Once the culture had reached *A*₅₇₈ ~ 4.0, the H₂/CO₂/H₂S (80%/20%/0.1%) was switched to H₂/CO₂ (80%/20%). 30 min after the H₂S gas flow was turned off, the CO₂/H₂ (20%/80%) was switched to 100% H₂. After purging for 20 min with 100% H₂ at 65 °C, the cells were cooled to ~20 °C within 10 min. After purging the cells with 100% H₂ for a total of 30 min, the cells were harvested anaerobically, and gas pressure was used to transfer the cells from the fermentor into a Cepa LE cell harvester (New Brunswick Scientific). After harvesting the cells, the rotor was immediately moved into the anaerobic chamber. The cells were removed from the rotor and resuspended in 200 ml (total volume) of 50 mM Tris-HCl, pH 7.6, 1 mM Ti(III) citrate, and 10 mM HSCoM (lysis buffer). The resuspended cells were aliquoted (50-ml aliquots) into four 100-ml serum vials (Alltech, Deerfield, IL) fitted with butyl rubber stoppers (Bellco Glass Inc., Vineland, NJ) and crimp-sealed with aluminum caps (Bellco Glass Inc.). The resuspended cells were placed under a 100% H₂ atmosphere by purging the headspace of the seal

serum vials with 100% H₂ for 5 min, followed by vigorously shaking the resuspended cells by hand for 30 s and then purging with 100% H₂ for an additional 5 min. The serum vials were inverted to minimize H₂ escape, and the cells were kept under 10 p.s.i. of 100% H₂ at room temperature with replacement of the H₂ atmosphere every 6–8 h. EPR spectroscopy was used to monitor *in vivo* generation of MCR_{red1} by drawing a 200-μl subsample of resuspended whole cells every 6–8 h. To remove trace amounts of oxygen in the H₂ line entering the anaerobic chamber, the line was fitted with a high pressure Oxy-Trap oxygen scrub (Alltech) followed by an indicating Oxy-Trap (Alltech) to monitor the efficiency/remaining capacity of the oxygen scrub. The cells were processed when the EPR intensity of MCR_{red1} stopped increasing, typically 24 h after cell harvest. MCR_{red1} and MCR_{ox1} were purified under strictly anaerobic conditions at 17 °C in a Vacuum Atmospheres chamber maintained below 1 ppm oxygen, monitored continually with a Teledyne oxygen analyzer (model 317; Teledyne Analytical Instruments, City of Industry, CA).

MCR_{ox1} was purified as described, except that methyl-SCoM was omitted from the lysis buffer (10). For experiments requiring high concentrations of MCR, MCR_{ox1} was concentrated in a 50-ml ultrafiltration stirred cell (Amicon; Millipore Corp., Bedford, MA) with a 30 kDa molecular mass cut-off filter using high pressure argon that had been passed through an oxisorb column (Oxyclear; Supelco) to remove oxygen.

MCR_{red1} used for the experiments presented in Figs. 2, 5, 8, 9, S1, and S2 was purified as described with the following modifications (10). The pellet from the 100% ammonium sulfate fractionation was resuspended in 60 ml of 50 mM Tris, pH 7.6, 10 mM HSCoM, 0.1 mM Ti(III) citrate (buffer A). The resuspended 100% ammonium sulfate pellet was applied at a flow rate of 5 ml/min to a 1.6 × 25-cm high performance Q-Sepharose (Sigma) column (C 16/40 column fitted with an AC 16 flow adapter (GE Health)) equilibrated in buffer A. After loading the resuspended pellet, the column was washed with 60 ml of buffer A, and protein was eluted with a step gradient of 0.44 M NaCl in buffer A (60 ml) followed by 0.55 M NaCl in buffer A (90 ml). Five-ml fractions were collected and analyzed for MCR_{red1} by UV-visible spectroscopy. MCR isoenzyme I typically eluted at the beginning of the 0.55 M NaCl step. The most concentrated fractions were transferred to separate 9-ml serum vials (Alltech) and stoppered with butyl rubber stoppers (Bellco). The serum vials were stored in the anaerobic chamber on ice packs in Styrofoam containers. In this way, MCR_{red1} can be stored in the anaerobic chamber for 3–4 months before losing all activity. This purification method routinely generates 50–80% MCR_{red1} as determined by UV-visible and EPR spectroscopy.

Spectroscopy of MCR—UV-visible spectra of MCR were recorded in the anaerobic chamber using a diode array spectrophotometer (model DT 1000A; Analytical Instrument Systems, Inc., Flemington, NJ). EPR spectra were recorded on a Bruker ESP 300E spectrometer recently upgraded to an EMX, equipped with an Oxford ITC4 temperature controller, a Hewlett-Packard model 5340 automatic frequency counter, and Bruker gaussmeter. Unless otherwise noted, the EPR spectroscopic parameters included the following: temperature, 100 K; microwave power, 10 milliwatts; microwave frequency, 9.43

GHz; receiver gain, 2×10^4 ; modulation amplitude, 12.8 G; modulation frequency, 100 kHz. Double integrations of the EPR spectra were performed and referenced to a 1 mM copper perchlorate standard. All NMR data were acquired at 298 K on a Bruker Avance DRX 500-MHz NMR instrument (Bruker Biospin Corp., Billerica, MA) equipped with a TXI cryoprobe in the UNL Chemistry Department.

Conversion of MCR_{ox1} to MCR_{red1} —For the experiments presented in Figs. 3, 4, 6, and 7, MCR_{ox1} was activated to the MCR_{red1} state in the absence of methyl-SCoM or HSCoM in a reaction mixture containing 20 mM Ti(III) citrate, 0.67 M TAPS (pH 10), 16.7 mM Tris-Cl (pH 7.6), and MCR (30–200 μ M). The mixture was heated at 60 °C for 40 min, cooled on ice, and then neutralized to pH 7.0–7.1 by adding an equal volume of 2 M Tris-HCl buffer (pH 7.0) (11). Protein concentrations were determined by the Bradford method using the Bio-Rad reagent and bovine serum albumin as a standard (38). F_{430} content was estimated using an extinction coefficient of 22,000 $\text{cm}^{-1} \text{M}^{-1}$ at 420 nm (39).

Conversion of MCR_{red1} to MCR_{PS} — MCR_{red1} used in Figs. 8, 9, and S1 was incubated for 5 min with a 10-fold excess of BPS in 50 mM Tris, pH 7.6. Unreacted BPS was removed from MCR_{PS} by buffer exchange using Amicon Ultra-15 centrifuge filter units with a 50 kDa cut-off (Millipore). Typically, 300–600 μ l of MCR_{PS} /BPS reaction mixture was exchanged into 3–6 ml of 50 mM Tris, pH 7.6. This mixture was concentrated to 200–300 μ l, and this process was repeated three times. The EPR spectroscopic parameters were as noted above except the following: temperature, 70 K; microwave power, 10.2 milliwatts; modulation amplitude, 5.0 G; scans, 4.

Measurement of MCR Activity—MCR assays were performed at 65 °C in rubber-sealed 8-ml serum vials. The standard assay mixture contained 20 mM methyl-SCoM, 1.2 mM HSCoB, 0.6 mM aquocobalamin, 25 mM Ti(III) citrate, and 0.5 M MOPS (pH 7.0) in a final volume of 0.4 ml. The reaction was started by increasing the temperature from 4 to 65 °C. The methane generated was determined by withdrawing gas samples at specific time points for analysis by gas chromatography (Varian model 3700 equipped with a flame ionization detector). Alternatively, MCR activity was measured by following the time-dependent loss of radioactivity as $^{14}\text{CH}_3\text{-SCoM}$ was converted to [^{14}C]methane (23). Rates of methane formation were calculated from the linear portion of the time course. One unit of MCR activity is equal to 1 μ mol of methane min^{-1} .

Reactions between MCR_{red1} and Sulfonates— MCR_{red1} (typically 0.1–0.2 mM) was incubated in 0.5 M TAPS (pH 10.0) for 10 min with various sulfonate-containing compounds at concentrations between 1 mM and 2 M: 2-bromoethanesulfonic acid sodium salt (BES), 2-(*N*-morpholino)ethanesulfonate (MES), BPS, 3-chloropropanesulfonyl chloride, CAPS, 3-mercapto-1-propanesulfonic acid sodium salt (Fluka), 4-bromo-1-butanethanesulfonic acid sodium salt (BBS), 4-chlorobutyric acid, 1-propanesulfonic acid sodium salt monohydrate (Fluka), 1-butanethanesulfonic acid sodium salt (Fluka), and MOPS. The formation of new complexes was identified by EPR.

Stopped-flow Studies—Stopped-flow experiments were performed on an Applied Photophysics spectrophotometer (SX.MV18; Leatherhead, UK) equipped with a photodiode

array detector. Constant temperature was maintained with a bath of nitrogen-bubbled water from a circulating pump to maintain anaerobicity. Rigorous measures were taken to purge oxygen from the stopped-flow instrument. The solutions of enzymes and inhibitors were made in the anaerobic chamber in 0.5 M TAPS, pH 10.0. The solutions were then loaded into tonometers, which had been incubated in the anaerobic chamber for 4 days and served as reservoirs for the drive syringes of the stopped-flow instrument. The drive syringes were maintained anaerobically at 25 °C in a temperature-controlled bath of anaerobic water. MCR_{red1} and varied concentrations of BPS were rapidly mixed at 25 °C in a 1:1 ratio. The reaction was monitored in the single wavelength mode by following the decay of MCR_{red1} at 388 and 715 nm, and MCR_{PS} formation was followed at 422 nm. Data were fit to single exponential decay functions with software provided by Applied Photophysics (version SX.MV.18). Reported rate constants are the average of at least five different rapid mixing experiments.

HPLC Connected to Conductivity Detector—The reaction between MCR_{red1} and BPS was initially followed by HPLC using a $3.9 \times 150\text{-mm}$ μ Bondapak C_{18} analytical column (Waters, Milford, MA), which was developed with a 0–80% methanol gradient in 10 mM ammonium formate (pH 3.3) (30 min at a flow rate of 1 ml/min). BPS decay was monitored using an absorbance detector set at 207 nm, whereas product formation was followed using a conductivity detector (Wescan Instruments Inc., Deerfield, IL). In this experiment, after activation in 0.5 M TAPS (pH 10.0), the MCR solution was exchanged with a solution containing 50 mM Tris-HCl (pH 7.6), 2 mM Ti(III) citrate using a 50-ml ultrafiltration stirred cell (Amicon) with a 30 kDa molecular mass cut-off. This step also removed any free F_{430} that could have been released from the enzyme during the activation step. The reaction was started by injecting 20 μ l of 0.5 M BPS solution (50 mM Tris-HCl, pH 7.6) into the 2-ml enzyme mixture. At each time point, 200 μ l of reaction mixture was removed, frozen in EPR tubes, and observed by EPR spectroscopy. Next, the enzyme solution was transferred to a 1.5-ml microcentrifuge tube and exposed to O_2 for 30 min. After diluting the sample with the same amount of Tris-HCl buffer, enzyme and ligands were separated by using microconcentrators (Amicon) with 30 kDa cut-off. The clear filtrate, which lacked MCR, was injected directly into the HPLC with the conductivity detector. The C_{18} column was pre-equilibrated with 50 mM formic acid (pH 3.0) and eluted with the same buffer at a flow rate of 0.5 ml/min. The retention times for BPS and PS were 6 and 5 min, respectively.

Chemical Quench Studies—Chemical quench experiments presented in Fig. 6 were performed at 20 °C using an Update Instruments (Madison, WI) chemical/freeze-quench apparatus with a model 745 controller. Rapid reaction kinetic studies were performed with MCR_{red1} and BPS in separate 2-ml stopped-flow syringes. Solutions of MCR_{red1} and BPS (both in buffer containing 50 mM Tris-HCl, pH 7.6, and 5 mM Ti(III) citrate) were rapidly mixed by activating the ram to displace each syringe by 1.3 mm, generating a total reaction volume of 82 μ l (41 μ l from each syringe) per shot. The ram speed was varied from 0.8 to 8.0 cm/s and was shown not to affect the observed reaction rate. Typically, a ram speed of 4.0 cm/s was used with

a 100-ms aging hose. For each data point, six shots were collected (492 μl) in an 18-ml scintillation vial containing 0.2 ml of 0.5 N formic acid. After the chemical quench experiment, each sample was lyophilized and dissolved in 100 μl of deionized water. The time course of each reaction was followed by monitoring the decrease in concentration of BPS and the formation of PS. The conditions and profile for eluting PS and BPS are the same as described above except that 80% methanol was used to wash out F_{430} from the column after each run. Data were fit to single exponential equations using Sigma Plot (Point Richmond, CA).

MCR_{red1} activity was measured prior to the rapid reaction kinetic experiments. The typical specific activity of the MCR used for the stopped-flow or chemical quench studies was 20–25 units/mg at 65 °C, which would be equivalent to 60–100 units/mg when corrected to 100% active MCR_{red1} . The amount of MCR_{red1} in each rapid reaction kinetic experiment was measured by double integration of the MCR_{red1} EPR signal before and after the stopped-flow or chemical quench experiments. Typical spin concentrations of the MCR_{red1} in the MCR samples for stopped-flow or chemical quench experiment ranged from 0.25 to 0.35 spin/mol of MCR, and less than 10% loss of this state occurred during the experiment.

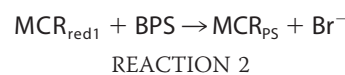
MCR_{red1} used in the chemical quench studies presented in Fig. 5 was prepared by removing HSCoM by buffer exchange exchanged into 50 mM Tris, pH 7.6, 0.1 mM Ti(III) citrate with Amicon Ultra-15 centrifuge filter units with a 50 kDa cut-off (Millipore). The concentration of MCR_{red1} was determined by UV-visible spectroscopy using extinction coefficients of 27.0 $\text{mm}^{-1} \text{cm}^{-1}$ and 9.15 $\text{mm}^{-1} \text{cm}^{-1}$ at 385 and 420 nm, respectively, using a multiple wavelength calculation (40). These values were established from a 100% MCR_{red1} sample as determined by EPR using a 1 mM copper perchloric acid standard. The concentration of $\text{MCR}_{\text{silent}}$ was calculated using extinction coefficients of 22.0 and 12.7 $\text{mm}^{-1} \text{cm}^{-1}$ at 420 and 385 nm, respectively (39). To ensure the accuracy of this method for determining the amount of MCR_{red1} in a solution containing a mixture of MCR_{red1} and $\text{MCR}_{\text{silent}}$ forms of the enzyme, the total protein concentration calculated with this method was compared with values determined using other methods. Protein concentrations calculated by this method were in good agreement (10–15%) with the Bio-Rad reagent (Bio-Rad) using bovine serum albumin as a standard. Total protein concentrations were also measured by converting a heterogeneous mixture containing $\text{MCR}_{\text{red1/silent}}$ to a homogeneous mixture containing 100% $\text{MCR}_{\text{silent}}$ by exposing it to air and using an extinction coefficient of 22.0 $\text{mm}^{-1} \text{cm}^{-1}$ to calculate the total MCR concentration (39).

Chemical quench experiments for Fig. 5 were performed with MCR_{red1} and BPS in separate 2-ml stopped-flow syringes. Solutions of MCR_{red1} and BPS were rapidly mixed by activating the ram to displace each syringe by 6.5 mm, generating a total reaction volume of 413 μl (206.5 μl from each syringe) per shot. A ram speed of 1.25 cm s^{-1} was used with a 500-ms aging hose. Each spectrum represents a total of 10 shots collected in a 30-ml serum vial (Alltech) containing 3 ml of 0.5 N formic acid to quench the reaction. After the reaction was quenched, enzyme and ligands were separated using a 50-ml ultrafiltration stirred

cell concentrator fitted with a 50 kDa cut-off filter (Millipore). To separate BPS/PS from other ligands, mainly F_{430} , the flow-through collected from the stirred cell was applied to a 2-ml C_{18} column equilibrated with water. The flow-through from the C_{18} column was collected and lyophilized to dryness and dissolved in 550 μl of 100% D_2O /0.75% 3-(trimethylsilyl)-propionic acid-D4 by weight for NMR analysis.

RESULTS

Reaction of MCR_{red1} with BPS and Related Analogs, Studied by EPR—BPS is the most potent known inhibitor of MCR (41). When MCR_{red1} is reacted with BPS, a unique EPR signal called “ MCR_{BPS} ” is observed, which, because of its air sensitivity and its similarity to the MCR_{red1} spectrum, was assigned as an Ni(I) state (42). A more recent study based on EPR data suggests that when MCR_{red1} reacts with BPS, bromide (or HBr) is presumably released, and a species is formed that can be described as an Ni(III)-propylsulfonate or a high spin Ni(II) with an alkylsulfonate radical (29). We confirmed this result (Table 1 and Fig. 2, inset) and have studied this reaction by various kinetic and spectroscopic methods (Reaction 2). Because the bromide has presumably undergone elimination, the designation “ MCR_{BPS} ” is misleading, and we use the designation “ MCR_{PS} ” instead. When MCR_{red1} is incubated with other structurally related sulfonates, an EPR signal nearly identical to MCR_{PS} is observed (Table 1) (29). Compounds that elicit this spectral change include 3-chloropropanesulfonyl chloride (1 mM) and BBS (7 mM) (Table 1). Unlike MCR_{ox1} and MCR_{red1} , these “ MCR_{PS} -like” EPR signals show no resolved hyperfine splitting, even when the modulation amplitude is decreased to 5.0 G. The MCR_{PS} signal is relatively stable in the absence of oxygen or one of the reagents that react with it (below), decaying with a half-life of ~ 8 h at pH 7.6 in the anaerobic chamber. However, in the presence of oxygen, the signal is rapidly quenched within 5 min).



The requirement for the sulfonate group of BPS to elicit the MCR_{PS} EPR signal was tested using 4-chlorobutyrate, in which a carboxylate group replaces the sulfonate. When reacted with MCR_{red1} , this BPS-like analog gave rise to an EPR signal nearly identical to MCR_{PS} . A similar result was reported earlier using 4-bromobutyric acid (29). However, reaction of MCR_{red1} with propanesulfonate (70 mM), butanesulfonate (70 mM), and 3-mercapto-1-propanesulfonate (90 mM) neither decreased the amount of the MCR_{red1} signal nor elicited any EPR spectral change. The reaction of MCR_{red1} with BES quenched the MCR_{red1} EPR signal, as reported previously (29) (Table 1).

We also tested the sulfonate-containing buffers MOPS, MES, CAPS, and CHES. Our initial data revealed that reacting MCR_{red1} with MOPS or CAPS gave the MCR_{PS} signal (data not shown). The buffer MES and CHES quenched the MCR_{red1} signal, like BES (data not shown). A caveat to these experiments is the relatively high concentrations of MOPS and CAPS to elicit the MCR_{PS} , 1.0 and 0.5 M, respectively. Further investigation led us to the description of the synthesis of these com-

TABLE 1

EPR signals generated from MCR_{red1} incubated with various BPS-like ligands

N/A, not applicable.

Chemical Name	Structure	EPR g values
I. Inhibitors that Quench MCR_{red1}		
2-Bromoethanesulfonate		N/A
3-Bromopropionate (29)		N/A
II. Inhibitors that induce the MCR_{PS-like} Signal		
3-x-propanesulfonate (x = Br, I (28, 29))		2.223, 2.115
3-chloropropanesulfonyl chloride		2.219, 2.114
4-Bromobutyrate (29)		2.219, 2.116
4-Chlorobutyrate		2.219, 2.096
4-Bromobutanesulfonate		2.216, 2.107
III. Compounds that do not react with MCR_{red1}		
3-Mercapto-1-propanesulfonate		N/A
1-Propanesulfonate		N/A
1-Butanesulfonate		N/A

pounds, BPS as a starting material for MOPS and CAPS and BES for MES and CHES (43). This would explain the high concentrations needed to elicit the MCR_{PS} signal, and the discrepancy in results from different batches of the same compound. For example, incubation of MCR_{red1} with 0.5 M of 98% pure CAPS at pH 7.0 elicited the MCR_{PS} EPR signal, whereas incubating with 0.5 M 99% pure CAPS at pH 7.0 did not. Therefore, we suggest that the EPR signals observed upon incubating MCR_{red1} with MOPS or CAPS and quenching of the EPR signal upon incubating with MES or CHES is due to contamination from the BPS or BES remaining in the starting material, respectively.

Reaction of MCR_{red1} and MCR_{PS} Formation, Followed by Rapid Kinetics—The UV-visible absorption spectra of EPR-active MCR_{PS} (Fig. 2) resemble those of EPR-active MCR_{ox1} and EPR-silent Ni(II) MCR_{silent} with absorbance maxima at 423 nm. In contrast, MCR_{red1} and Ni(I)F₄₃₀ exhibit a 40-nm blue shift relative to the MCR_{PS}, MCR_{ox1}, and Ni(II) forms, which suggest that BPS causes a redox change in MCR. We followed the reaction of MCR_{red1} with BPS by absorption spectroscopy using a stopped-flow instrument (Fig. 3). Single exponential kinetics are observed although the reaction is not run under pseudo-first order conditions. Decay of the MCR_{red1} absorbance peaks at 388 and 715 nm matches the rate of formation of the MCR_{PS} absorbance peak at 422 nm. This indicates that there is no intermediate between the MCR_{red1} and MCR_{PS} states; alternatively,

any intermediate that is formed is too transient to be observed. On the basis of the BPS concentration dependence of the UV-visible spectral changes (Fig. 4), the second order rate constant for MCR_{PS} formation (or MCR_{red1} decay) is $1.6 \times 10^5 \text{ M}^{-1} \text{ s}^{-1}$ (at 20 °C). This value is about 10-fold higher than the k_{cat}/K_m for methyl-SCoM ($1.9 \times 10^4 \text{ M}^{-1} \text{ s}^{-1}$ at 65 °C) and 100-fold larger than the k_{cat}/K_m for HSCoB ($2.2 \times 10^3 \text{ M}^{-1} \text{ s}^{-1}$; 20 °C) in methane formation (23). The rate constants at pH 7.6 (in 50 mM Tris-HCl) buffer are identical to those at pH 10.0 (in 0.5 M TAPS) (data not shown).

MCR_{red1} can also react with BBS but with significantly lowered efficiency. As shown in Fig. S2 (see supplemental material), the kinetic parameters for formation of MCR_{BS} (in analogy with MCR_{PS}) and MCR_{red1} decay are as follows: $k_{\text{max}} = 21.4 \pm 0.3 \text{ s}^{-1}$, $K_m = 9.4 \pm 0.3 \text{ mM}$, $k_{\text{max}}/K_m = 2270 \pm 70 \text{ M}^{-1} \text{ s}^{-1}$. Thus, the second order rate constant for reaction between MCR_{red1} and BBS is about 70-fold lower than that for reaction with BPS. In the case of BBS, the electrophilic carbon adjacent to the bromide leaving group is five bonds (~6 Å) from the sulfonate group, which corresponds to the methyl group of methyl-SCoM.

Reaction of MCR_{ox1} with BPS—When MCR_{ox1} was incubated with BPS in the absence of Ti(III) citrate for several hours at room temperature, the MCR_{PS} EPR signal appeared. The spectrum of MCR_{PS} formed from MCR_{ox1} is indistinguishable from that formed from MCR_{red1}, yet the second order rate constant

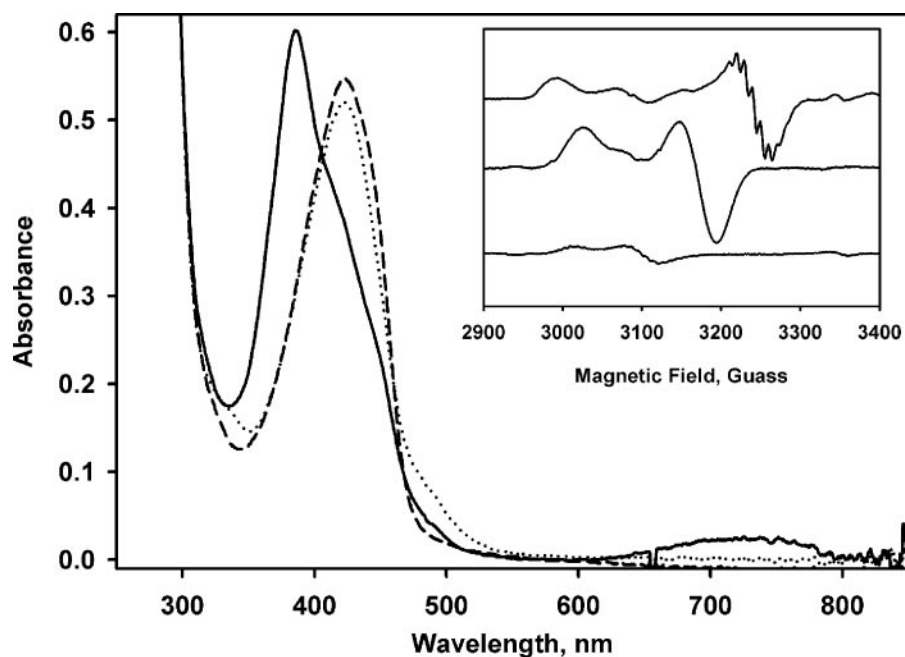


FIGURE 2. UV-visible spectral changes associated with reaction of MCR_{red1} with BPS. MCR_{red1} ($20 \mu\text{M}$ (solid line)) was incubated with $200 \mu\text{M}$ BPS in 50 mM Tris (pH 7.6) at 20°C (dotted line). MCR_{PS} formed was exposed to air for 10 min until the EPR signal (see inset) of MCR_{PS} was totally quenched (dashed line). Inset, representative EPR spectra of MCR_{red1} (top), MCR_{PS} (middle), and MCR_{PS} exposed to air (bottom). Note that the EPR signal in the bottom spectrum is not MCR_{PS} but contaminating MCR_{ox1} , which is also seen in the spectra of MCR_{red1} and MCR_{PS} .

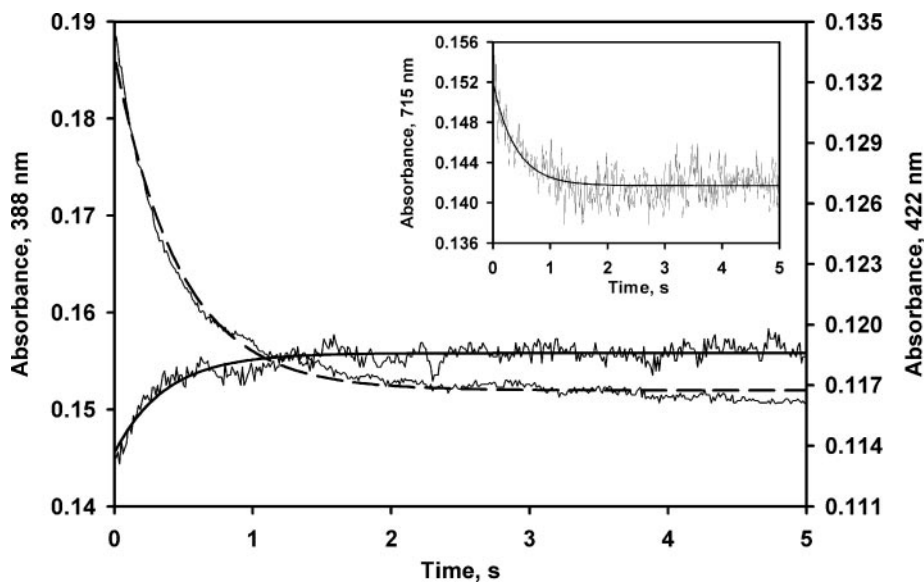


FIGURE 3. Stopped-flow reaction of MCR_{red1} with BPS. MCR ($10 \mu\text{M}$ with 0.22 spins/mol of MCR_{red1}) was mixed with $30 \mu\text{M}$ BPS at room temperature. The data were fit with a single exponential equation. The rate constants were determined as follows: $2.15 \pm 0.03 \text{ s}^{-1}$ (388 nm ; dashed line); $2.72 \pm 0.14 \text{ s}^{-1}$ (422 nm ; solid line); $2.50 \pm 0.22 \text{ s}^{-1}$ (715 nm ; inset).

($2.4 \text{ M}^{-1} \text{ s}^{-1}$) (19) is 10^5 -fold slower than that for formation of MCR_{PS} from MCR_{red1} (see above). This suggests, as proposed earlier (44), that the reactivity of MCR_{ox1} may be due to a very low amount (as low as 0.001% ; i.e. $1/10^5$) of MCR_{red1} present in the MCR_{ox1} solution. Such low amounts would be undetectable by any spectroscopic method. The rate of MCR_{ox1} decay matches the rate of MCR_{PS} formation, and these rates are faster at pH 10.0 than at pH 7.6 (data not shown) (40), which also would be consistent with MCR_{red1} intermediacy in this process,

since pH 10.0 is optimal for activation of MCR_{ox1} to MCR_{red1} with Ti(III) citrate (45). Furthermore, as described above, formation of MCR_{PS} involves oxidation of MCR_{red1} to an “ MCR_{ox1} -like” state and reduction of BPS (see above). Thus, the data indicate that MCR_{red1} , but not MCR_{ox1} , can generate the MCR_{PS} state.

MCR_{red1} -catalyzed Propanesulfonate Formation from BPS—As noted above, the similarity between the UV-visible and EPR spectra of MCR_{PS} and MCR_{ox1} indicates that MCR_{red1} is two electrons more reduced than MCR_{PS} . The EPR spectra generated when MCR_{red1} is reacted with 3-iodo- or 3-chloropropanesulfonate is identical to MCR_{PS} with no detectable hyperfine splitting from bromide or iodine (28), indicating that the halogen has been eliminated during formation of the MCR_{PS} species. Rapid chemical quench methods were used to identify the alkylsulfonate group that is proposed to ligate to nickel (see Scheme 1). It was expected that quenching the reaction in acid would protonate the propylsulfonate ligand (forming HPS) and inactivate MCR. We removed HSCoM from the solution containing MCR_{red1} (MCR_{red1} is usually stored in the presence of HSCoM , because it stabilizes this form of the enzyme), because thiolates react directly with BPS in the absence of MCR. MCR_{red1} was rapidly mixed with BPS (in the absence of HSCoB and HSCoM) under single turnover conditions in the chemical quench apparatus, and the reaction was quenched into a solution containing 0.5 M formic acid. Then the small molecule products were separated from the protein by ultrafiltration and analyzed by NMR

spectroscopy to measure the appearance of the product of this reaction. When MCR_{red1} and Ti(III) citrate (in a 2.4- and 1.4-fold molar excess of the BPS, respectively) were reacted with BPS, HPS was detected as the product of the acid quench (Reaction 3; Fig. 5A). The reaction has a strict requirement for MCR_{red1} , since, when MCR_{red1} was omitted and Ti(III) citrate was present in a 2.9-fold molar excess (relative to BPS), the HPS peaks were absent, whereas peaks characteristic of BPS remained (Fig. 5B). Furthermore, when the $\text{MCR}_{\text{silent}}$ form of

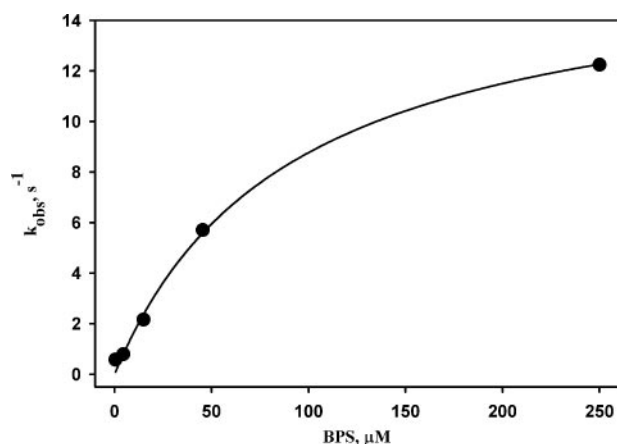
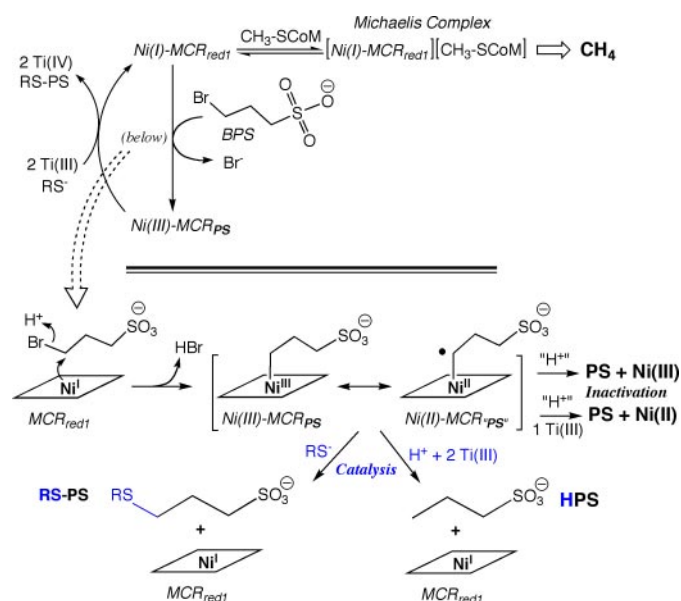
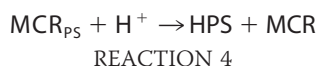
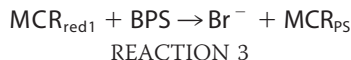


FIGURE 4. Dependence of k_{obs} for MCR_{PS} formation on BPS concentration. MCR ($10\ \mu\text{M}$ with 0.22 spins/mol of MCR_{red1}) was mixed with different concentrations of BPS at room temperature. The data were fit with a hyperbolic equation ($k_{\text{max}} = 16.7 \pm 0.7\ \text{s}^{-1}$, $K_m = 90 \pm 10\ \mu\text{M}$).



SCHEME 1. Reaction of MCR_{red1} with BPS: catalysis versus inactivation.

the enzyme was rapidly reacted with BPS under similar conditions, PS was not detected as a product (data not shown). These results demonstrate that the reaction of MCR_{red1} with BPS leads to debromination and formation of a propylsulfonate adduct (MCR_{PS} ; Reaction 3) that can undergo protonolysis to form propanesulfonate (HPS; Reaction 4).



To determine the rate of propylsulfonate adduct formation relative to the rate of MCR_{PS} generation (as measured by UV-visible and EPR spectroscopy), the MCR_{red1} -catalyzed conversion of BPS to PS was monitored under single turnover conditions by rapid chemical quench methods (quenched with formic acid). HPS formation and BPS depletion were measured by HPLC connected to a conductivity detector (Fig. 6). The

product was identified by its elution at the same position as an authentic HPS standard. The rates and amplitudes for BPS decay and HPS formation were identical and equaled the rates of MCR_{PS} formation and MCR_{red1} decay (above in Fig. 3).

These combined results indicate that the reaction of MCR_{red1} with BPS occurs according to Reaction 3 (*i.e.* the oxidation of MCR_{red1} is coupled to reduction of BPS to form MCR_{PS} , which undergoes protonolysis to form propanesulfonate). Propanesulfonate appears to be the only product formed from BPS, as summarized in Scheme 1.

Evidence that MCR_{PS} Can Be Reactivated to MCR_{red1} —The results described above demonstrate that Ni(I) of MCR_{red1} performs a nucleophilic attack on BPS to form MCR_{PS} and bromide. This is an oxidative addition, much like the methyltransferase-catalyzed reaction of cob(I)alamin with $\text{CH}_3\text{-H}_4\text{-folate}$ to form methyl-cob(III)alamin and $\text{H}_4\text{-folate}$ (46). The reaction of MCR with BPS has been thought to lead to irreversible inactivation of MCR. However, NMR results indicate that multiple turnovers of BPS conversion to propanesulfonate can occur.

PS formation was followed by HPLC under multiple turnover conditions in which MCR_{red1} was incubated with a 100-fold excess of BPS (Fig. 7). MCR_{red1} acts as a catalyst in this reaction, since the amount of propanesulfonate formed is 11-fold greater than the amount of enzyme. There are two major differences between the results of the steady-state reaction (Fig. 7) and the single turnover reaction (Fig. 6). The k_{obs} for the single turnover reaction ($2.6\ \text{s}^{-1}$) (Fig. 6), which equals the rate constant for formation of MCR_{PS} (Figs. 4 and 5), is much faster than the steady-state rate ($2.2\ \text{h}^{-1}$, calculated based on either the exponential (k_{obs}) or the initial velocity (linear portion) in Fig. 7) of propanesulfonate formation, indicating that it is not chemistry but rather regeneration of MCR_{red1} or propanesulfonate release that is rate-limiting in the steady-state reaction. In addition, in the single turnover reaction, BPS is fully converted to propanesulfonic acid, whereas in the steady-state reaction, only 10% conversion occurs. This indicates that MCR_{red1} or MCR_{PS} undergoes slow inactivation by conversion to a Ni(II) MCR-silent state during the steady state reaction. Thus, as shown in Scheme 1, MCR_{PS} can suffer two alternative fates: reactivation to form MCR_{red1} or inactivation to form a Ni(II) silent state (or potentially a Ni(III) state). Furthermore, comparison of the steady-state and transient kinetics experiments provides strong evidence that the MCR_{PS} state is a catalytically competent intermediate in propanesulfonate formation.

Reaction of MCR with BPS and Reversibility of MCR_{PS} Formation—The catalytic conversion of BPS to propanesulfonate requires that the active MCR_{red1} state be regenerated from MCR_{PS} at each catalytic cycle (Scheme 1). Ti(III) citrate was capable of supporting the steady-state reaction, indicating that reductive activation is required for the cycling of MCR between the MCR_{PS} and MCR_{red1} states.

Since HSCoB can donate electrons for methane formation from methyl-SCoM, we tested whether HSCoB could also regenerate MCR_{red1} from MCR_{PS} . In methane formation, the product is CoBS-SCoM. In this case, we would expect to form CoBS-PS. However, HSCoB was unable to reactivate MCR_{PS} to MCR_{red1} . On the other hand, various small thiolates, including CoMSH, did convert MCR_{PS} to MCR_{red1} . To better understand

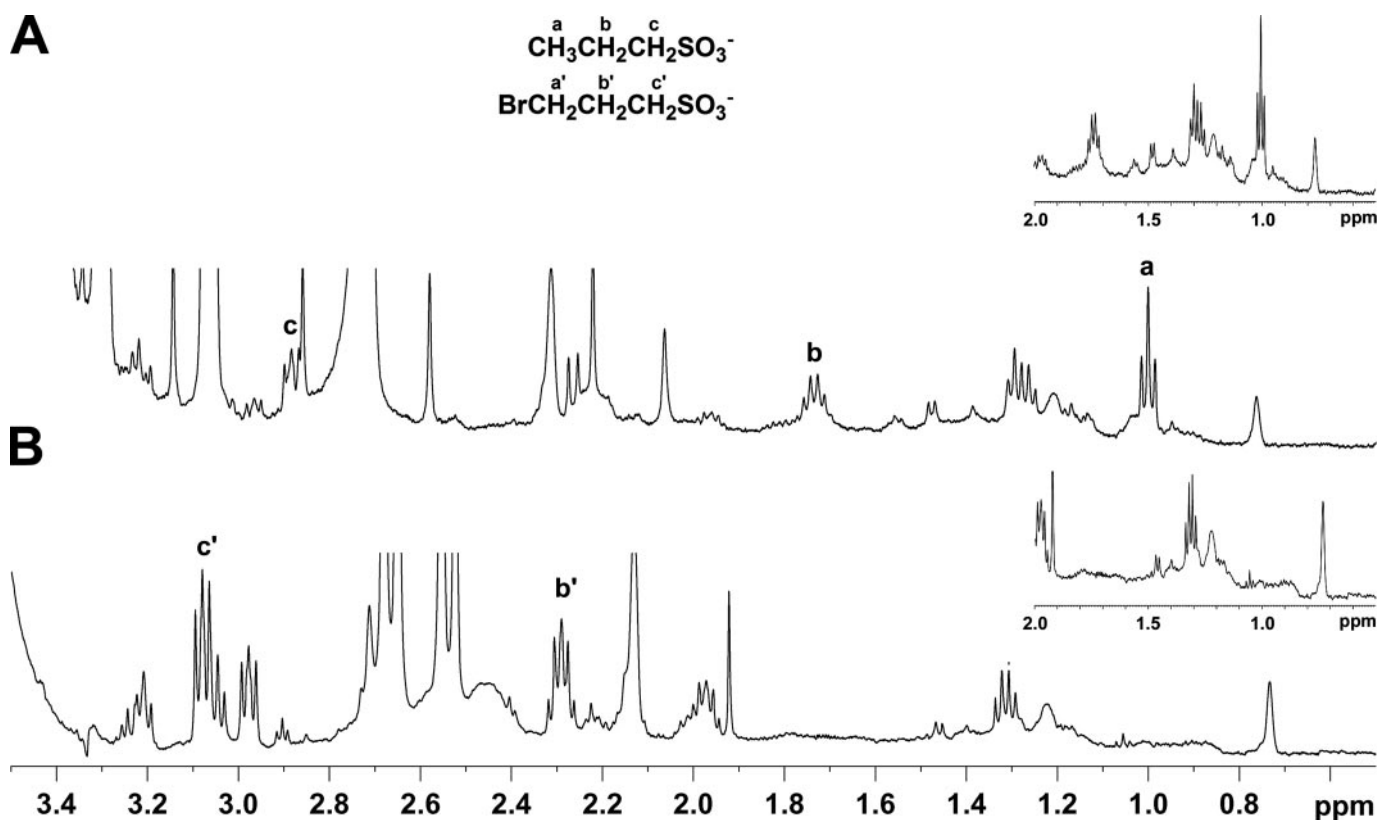


FIGURE 5. ^1H NMR evidence for propanesulfonate formation from MCR_{red1} and BPS. A, a solution containing 0.169 mM MCR_{red1} and 0.1 mM Ti(III) citrate in 50 mM Tris, pH 7.6 (syringe 1) was reacted with 0.069 mM BPS in 50 mM Tris, pH 7.6 (syringe 2). B, a solution containing 0.2 mM Ti(III) citrate in 50 mM Tris, pH 7.6 (syringe 1) was reacted with 0.069 mM BPS in 50 mM Tris, pH 7.6, in the absence of MCR. ^1H chemical shifts for PS and BPS as determined by pure standards were as follows: 1.02(t), 1.75(m), and 2.90(t); 2.29 (m), 3.08(t), and 3.61(t) ppm, respectively. In B, the BPS signal at 3.61 ppm was not seen due to overlap with the solvent peak. The insets in A and B show the 0.5–2.0 ppm region. See “Experimental Procedures” for chemical quench program details and sample processing for NMR analysis.

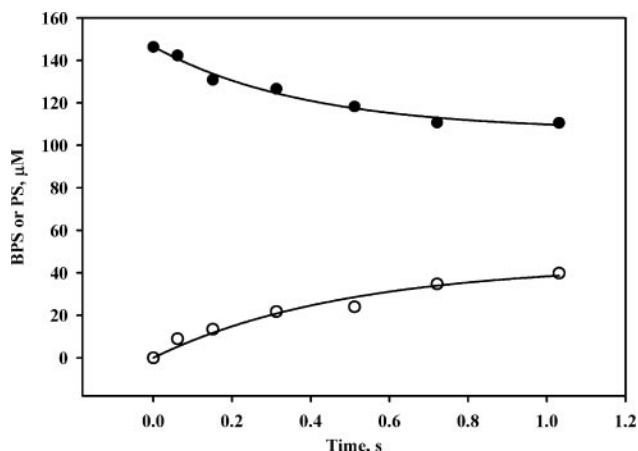


FIGURE 6. Rapid chemical quench studies of the reaction of MCR_{red1} with BPS. A solution containing 90 μM MCR_{red1} (in 50 mM Tris-HCl buffer, pH 7.6) was rapidly mixed with 300 μM BPS (150 μM , final) 50 mM Tris-HCl buffer, pH 7.6) at 20 $^\circ\text{C}$. The decay of BPS (solid circle) and the formation of PS (open circle) were monitored by using HPLC connected to a conductivity detector. The rate constants, $2.6 \pm 0.6 \text{ s}^{-1}$ for BPS decay and $2.0 \pm 0.6 \text{ s}^{-1}$ for PS formation and the amplitudes $19.5 \pm 1.7 \text{ nmol}$ ($39.7 \pm 3.4 \mu\text{M}$) and $21.6 \pm 2.9 \text{ nmol}$ ($44.0 \pm 5.8 \mu\text{M}$) for BPS and for PS, were determined by fitting the data to single-exponential equations.

the reaction of MCR_{PS} with HSCoM, we monitored the reaction by EPR (Fig. S1) and UV-visible spectroscopy (Fig. 8). Conversion of MCR_{PS} to MCR_{red1} in the presence of HSCoM was determined by following the decrease of MCR_{PS} at 420 nm and

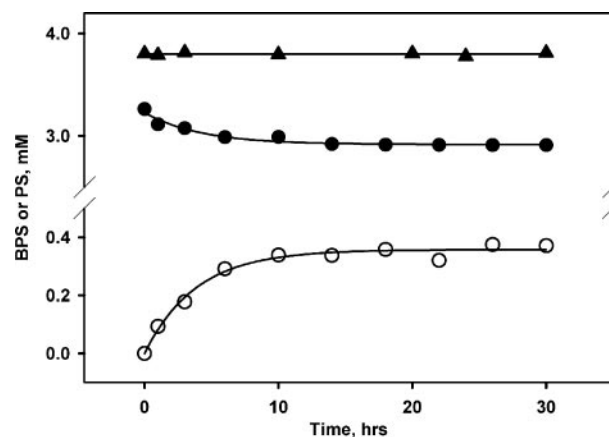


FIGURE 7. Steady-state reaction of MCR_{red1} with BPS. BPS decay (solid circle, amplitude = $0.31 \pm 0.03 \text{ mM}$, $k_{\text{obs}} = 0.24 \pm 0.05 \text{ h}^{-1}$) and propanesulfonate formation (open circle, amplitude = $0.36 \pm 0.01 \text{ mM}$, $k_{\text{obs}} = 0.26 \pm 0.03 \text{ h}^{-1}$) when 33 μM MCR_{red1} (in 5 mM Ti(III) citrate) was reacted with 3.0 mM BPS in 50 mM Tris-HCl (pH 7.6). BPS and propanesulfonate were detected by reverse phase HPLC connected to a conductivity detector. The rate constants and the amplitudes were determined by fitting the data to single-exponential equations. There is no decay of BPS when MCR is excluded from the reaction mixture (triangle).

increase of MCR_{red1} at 385 nm. At HSCoM concentrations between 0.2 and 4 mM, $\sim 80\%$ conversion of MCR_{PS} to MCR_{red1} was achieved (data not shown). The remaining 20% of MCR_{PS} probably decays into $\text{MCR}_{\text{silent}}$, which is indistinguishable from MCR_{PS} by absorption spectroscopy but is EPR-silent. The rate

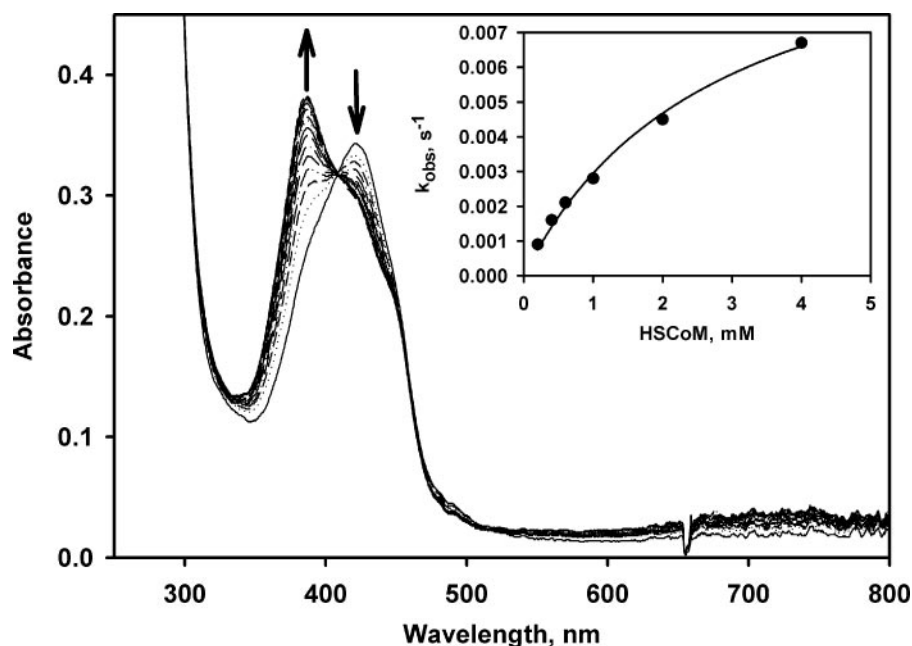


FIGURE 8. **MCR_{red1} “reactivation” from MCR_{PS}.** MCR_{PS} (12.2 μ M) was incubated with 4 mM HSCoM, 0.5 M TAPS buffer (pH 10.0) at 25 °C. The decay of MCR_{PS} (420 nm) and the formation of MCR_{red1} (385 nm) were followed by UV-visible spectroscopy; each spectrum represents a 30-s time interval. The rate constants (0.0067 ± 0.0001 s⁻¹ for MCR_{PS} and 0.0067 ± 0.0004 s⁻¹ for MCR_{red1}) were obtained by fitting the data with single exponential equations. *Inset*, the second order rate constant 3.99 ± 0.65 M⁻¹ s⁻¹ (k_{max} 0.011 ± 0.001 s⁻¹ and K_m 2.81 ± 0.40 mM) was calculated by plotting first order rates versus various HSCoM concentrations while keeping the MCR_{PS} concentration constant and fitting the data with a two-parameter hyperbolic equation.

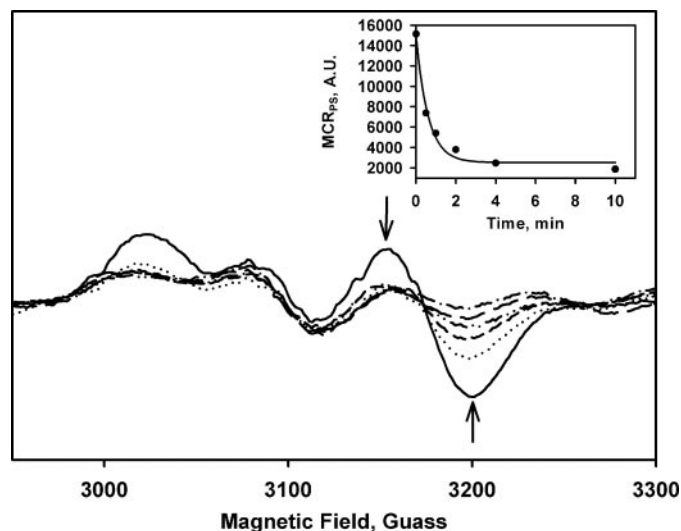


FIGURE 9. **MCR_{PS} is converted to MCR_{silent} in the presence of Ti(III) citrate.** Shown is MCR_{PS} (20 μ M) in 500 mM TAPS buffer (pH 10) (solid line) and 30 s (dotted line) to 10 min (dotted and dashed line) after incubating with Ti(III) citrate (400 μ M) at 25 °C. The arrows indicate the direction of change for the MCR_{PS} signal after adding Ti(III) citrate. *Inset*, the rate constant for MCR_{PS} decay was fit to a single exponential equation ($k_{\text{obs}} = 1.63 \pm 0.26$ min⁻¹).

of MCR_{PS} conversion to MCR_{red1} was dependent on the concentration of HSCoM with a second order rate constant of 3.99 M⁻¹ s⁻¹ (Fig. 8, *inset*), which is about 40,000-fold slower than the second order rate constant for MCR_{PS} formation (1.6×10^5 M⁻¹ s⁻¹). This large difference between the second order rate constants for the formation of MCR_{PS} versus “reactivation” by forming MCR_{red1} was crucial in our ability to characterize MCR_{PS} as an intermediate in PS formation. This rate mismatch

also is what led to the earlier assignment of BPS as an irreversible inhibitor. The slow rate of reactivation of MCR_{PS} to MCR_{red1} also indicates that the steady-state rate of PS formation will be very slow (as is shown below), because the multiple turnover reaction will be limited by the reactivation rate constant.

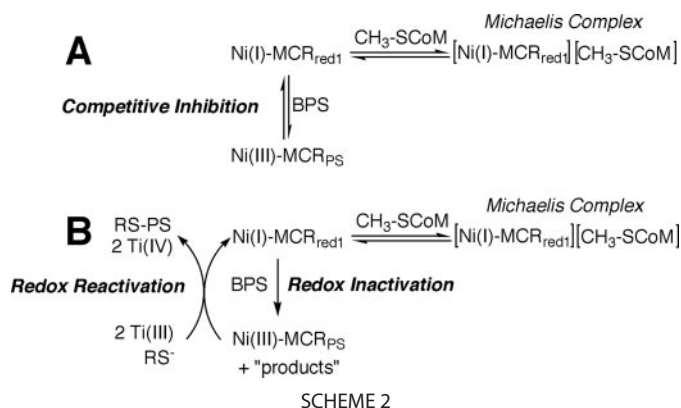
Ti(III) citrate is less efficient than CoMSH in converting MCR_{PS} to MCR_{red1}. Within 10 min at pH 10, Ti(III) citrate converted only ~5% MCR_{PS} to MCR_{red1}, whereas ~83% MCR_{PS} converted to an EPR-silent form of the enzyme, and ~12% remained as MCR_{PS} (Fig. 9). At pH 7.6, MCR_{PS} was unaffected by Ti(III) citrate over the same period of time (data not shown).

The HSCoM-dependent conversion of MCR_{PS} to MCR_{red1} is pH-dependent, showing no conversion at pH 7.2 (data not shown). In an experiment otherwise identical to the one described in Fig. 8, 4 mM MeSCoM was used in place of HSCoM; under these conditions, MCR_{PS} was not reactivated to MCR_{red1} (data not shown), demonstrating the importance of the thiol group of HSCoM for reactivation. A survey of thiols has not been performed; however, dithiothreitol and mercaptoethanol were found to reactivate MCR_{PS}.

As summarized in Schemes 1 and 2, these results indicate that BPS is not a competitive inhibitor or irreversible inactivator but rather a reversible redox inactivator of MCR (reversible by HSCoM) that can serve as an alternative substrate and that MCR_{PS} is a more oxidized state than MCR_{red1}, which can be converted back to the MCR_{red1} state by thiolate nucleophiles or, less efficiently, by Ti(III) citrate.

DISCUSSION

BPS has been described as a highly potent competitive inhibitor (apparent $K_i = 50$ nM) (41) and as an irreversible inhibitor (44) of MCR, and its high affinity has been exploited to titrate the active sites of this enzyme (11, 47). Here we clarify the reaction of the active MCR_{red1} state with BPS by a combination of spectroscopic and kinetic studies. As shown in Schemes 1 and 2, this reaction occurs by the nucleophilic attack of Ni(I) on BPS to displace bromide and generate the EPR-active MCR_{PS} species. MCR_{PS} (formerly called MCR_{BPS}) was described by Rospert *et al.* (28) and assigned as a high spin Ni(II)-alkylsulfonate radical species (29, 48). The lack of detectable hyperfine broadening from the halide of BPS (or any of the related compounds shown in Table 1 that give the MCR_{PS} signal) provided evidence that the bromide undergoes elimination before or as the MCR_{PS} state is formed. In fact, identical EPR spectra (MCR_{PS}) are formed by incubating MCR_{red1} with 3-bromo- ($I = 3/2$), and 3-iodo- ($I = 5/2$) propanesulfonate with no



detectable hyperfine splitting from these halide atoms, indicating that the nickel is not positioned close to the halogen groups of these ligands (28). Advanced EPR studies have defined the hyperfine coupling constants between the Ni(III) center and the alkyl ligand; however, in this complex, 75% of the spin is in the nickel $d_{x^2-y^2}$ orbital and ~7% on the attached methylene carbon atom (48). These values are in reasonable agreement with a DFT calculation on a methyl-Ni(III)-F₄₃₀ model (49).⁶

In the studies described here, MCR_{red1} was reacted with BPS, and the propylsulfonate ligand was unambiguously identified (after acid quenching) as propanesulfonate by NMR spectroscopy and by HPLC analysis in both single and multiple turnover reactions. This experiment would not *per se* rule out the possibility that the various halopropane sulfonates ligate to nickel via the sulfonate oxygen(s), especially since similar MCR_{PS}-like EPR spectra are generated when MCR_{red1} is incubated with bromobutanesulfonate and chloropropane sulfonate (Table 1). However, other sulfonates, including 3-mercapto-1-propanesulfonic acid, butanesulfonate, and propanesulfonate, do not induce MCR_{PS}-like EPR signals. Furthermore, the reaction of MCR_{red1} with 4-bromobutyric acid (29) or 4-chlorobutyric acid generates an EPR signal nearly identical to MCR_{PS}. Therefore, the sulfonate group is not a strict requirement for generation of the MCR_{PS} signal, only its anionic character. In addition, the advanced EPR studies described above strongly indicate the formation of an organometallic alkyl-nickel species (49).

Besides its intermediacy in PS formation from BPS, MCR_{PS} is interesting in sharing some striking similarities to the MCR_{ox1} state. These two states are functionally similar in that they can be activated to the MCR_{red1} state⁷; however, it has so far proven impossible to activate other Ni(II) states of MCR. The “ready” nature of the MCR_{PS} and MCR_{ox1} states must be related to their electronic structures, which have both been assigned as Ni(II) associated with a radical, a thiyl radical in the case of MCR_{ox1} (15, 17) and an alkylsulfonate radical for MCR_{PS} (29). The UV-visible spectra of these two species are indistinguishable, indicating that MCR_{ox1} and MCR_{PS} share the same nickel oxidation state. The EPR spectra are similar (for MCR_{ox1}, the *g* values are 2.231, 2.153, and for MCR_{PS}, they are 2.223, 2.115), which would be consistent with the two species sharing the same oxi-

dation state but different coordination states. Since the four planar nitrogens of the macrocycle are unlikely to vary, the spectral differences must result from changes in the upper axial ligands: a thiyl radical for MCR_{ox1} versus an alkyl radical in the case of MCR_{PS}.

In the presence of the low potential reductant Ti(III) citrate, the MCR_{PS} state undergoes reductive activation and protonolysis to form MCR_{red1} and propanesulfonic acid. Some thiolates like HSCoM, dithiothreitol, and mercaptoethanol also react with MCR_{PS} to regenerate MCR_{red1} and presumably a thioether product, whose characterization is under way. Thus, BPS can serve as an alternative substrate for MCR. In these reactions, the rate of MCR_{PS} formation ($k_{\text{max}}/K_m = 190 \text{ mM}^{-1} \text{ s}^{-1}$, $k_{\text{max}} \sim 17 \text{ s}^{-1}$ at 20 °C) is ~60-fold faster than the rate of methane formation from the natural substrates, methyl-SCoM and HSCoB ($k_{\text{cat}}/K_m = 3 \text{ mM}^{-1} \text{ s}^{-1}$ at 20 °C, 50 mM s^{-1} at 60 °C (23)). However, the elimination of PS and regeneration of MCR_{red1} occurs 1000-fold more slowly than methane formation from the natural substrates. The large difference between the rates of MCR_{PS} formation and regeneration of MCR_{red1} explains the nearly stoichiometric accumulation of MCR_{PS} and rationalizes why BPS acts as such a strong inhibitor of MCR.

Schemes 1 and 2 rationalize the seemingly disparate properties of BPS, which have led to its classification as a competitive inhibitor (41), as an irreversible inhibitor (44), and, as described here, as an alternative substrate and a redox inactivator. Based on steady-state kinetics, BPS would appear to be a competitive inhibitor, because the active enzyme (MCR_{red1}) can react either with BPS or methyl-SCoM and because there is a path from MCR_{PS} back to active MCR_{red1}. Therefore, in comparing the competitive inhibition Mechanism A with the redox inactivation/reactivation Mechanism B (Scheme 2), as long as the reactivation of MCR_{red1} is rapid and complete (*i.e.* the enzyme rapidly and quantitatively returns to its active state), one would not suspect the occurrence of a series of complex underlying reactions. However, by following enzyme-monitored turnover reactions, it is clear that BPS is not a traditional competitive inhibitor in a simple rapid equilibrium with free enzyme nor an irreversible inactivator, because there is a redox pathway back to the active enzyme form.

These results demonstrate conclusively that the MCR_{PS} state is a catalytically competent intermediate in propanesulfonate formation and constitute the first spectroscopic observation of any intermediates in the MCR reaction that can be related to catalysis. The results could thus be considered to support the intermediacy of an alkylnickel intermediate in MCR-catalyzed methane formation from methyl-SCoM. In the rest of this discussion, the results are discussed in relation to Mechanisms I and II.

With respect to Mechanism I, the formation of the MCR_{PS} intermediate at rates exceeding the rate of methane formation from methyl-SCoM indicates the possibility that an alkylnickel intermediate is involved in methanogenesis. Furthermore, any reaction mechanism must exhibit the property of microreversibility; therefore, as shown in Fig. 11, our results provide evidence for an alkylnickel intermediate in the final step of anaerobic methane oxidation. According to Mechanism I (Fig. 11A), this step involves the thiolytic cleavage of an alkylnickel bond to

⁶ The DFT calculations predict 76% spin on Ni(III) and no detectable spin on the methyl carbon.

⁷ As shown above, Ti(III) citrate can reduce MCR_{ox1} and MCR_{PS} to the MCR_{red1} state and HSCoM can reduce MCR_{PS} to the MCR_{red1} state.

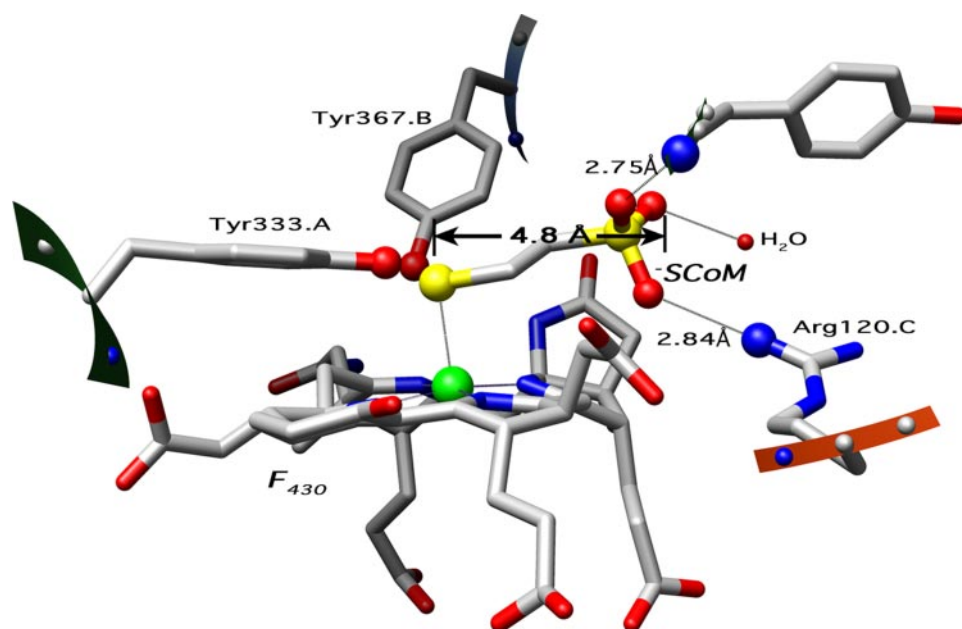


FIGURE 10. **Interactions of CoM with MCR.** This structure was generated using the program Chimera based on Protein Data Bank identifier 1HBU (13).

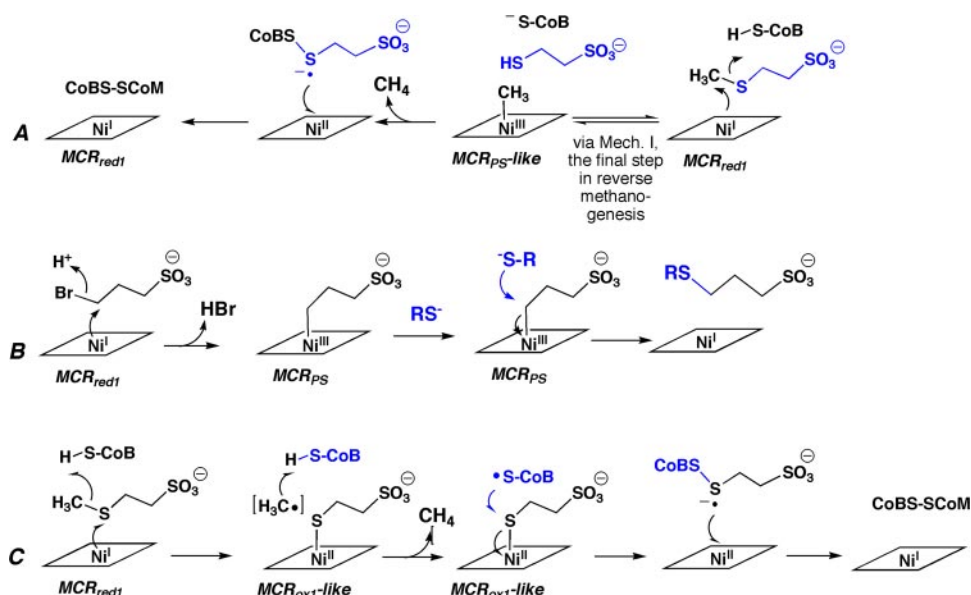


FIGURE 11. **Proposed mechanisms of reaction of MCR_{red1} with BPS (B) and methyl-SCoM according to Mechanism I (A) and Mechanism II (C).** C is based on the proposal by Siegbahn and co-workers (27, 50).

form the thioether, methyl-SCoM, and regenerate MCR_{red1} . Then proton transfer to the methyl group to form methane, followed by electron transfer to Ni^{III} to generate Ni^{II} , would generate a disulfide anion radical, which is considered to be sufficiently reducing to convert Ni^{II} back to the active MCR_{red1} state.

On the other hand, the relationship of the alkylnickel intermediate to Mechanism I deserves a few words of caution, since the properties of methyl-SCoM and BPS are quite different. Although the strength of the $\text{CH}_3\text{-SCoM}$ bond (293 kJ/mol (27)) is similar to that of the C-Br bond in BPS (~ 270 kJ/mol), neither the methyl group (if Ni^{I} attacked the thioether sulfur) nor the mercaptoalkylsulfonate group (CoMS^-) (if nickel attacked the methyl group) of methyl-SCoM is a good leaving

group. However, bromide is an excellent leaving group. The standard measure of the goodness of a leaving group is the pK_a of its conjugate acid (HBr versus CH_4); the lower the pK_a , the better the leaving group ability. Methane is one of the weakest acids known, with a pK_a of 50, whereas HBr is a very strong acid, with a pK_a of -9 . HSCoM would have an intermediate pK_a of around 8. Therefore, an ionic reaction of MCR_{red1} with BPS to eliminate bromide and form Ni^{III} -alkylsulfonate is quite reasonable; however, it is unlikely that Ni^{I} reacts with methyl-SCoM to eliminate a methyl anion and form Ni^{III} -SCoM or to eliminate SCoM^- and form methyl- Ni^{III} . Furthermore, computational results suggest that cleavage of a high energy methyl-SCoM (~ 70 kcal/mol) bond to form a weak methyl-nickel (less than 25 kcal/mol) bond is thermodynamically unreasonable, and a radical mechanism (Fig. 11C) was proposed that involves reaction of Ni^{I} with the sulfur of methyl-SCoM to generate a Ni^{II} -thiolate and a methyl radical, which abstracts a hydrogen atom from HSCoB (27, 50).

The role of HSCoB in the MCR reaction was assessed by single turnover kinetic studies using the chemical quench technique with radioactive [^{14}C -methyl]SCoM as the substrate. These transient kinetic studies demonstrated that formation of even a single equivalent of methane requires HSCoB (23). This reaction was repeated with an analog of HSCoB that is one

carbon shorter in length (mercaptoHEXanoyl-threonine phosphate). A single exponential decay was observed in both reactions that depended on the concentration on HSCoB or the analog, which was shown to react 1000-fold slower than HSCoB . These results indicate that HSCoB is not required for proton donation, since the acidic conditions of the quench would have supplanted that role by protonolysis of the methyl-nickel intermediate to form methane and indicate that HSCoB has an integral role in a step(s) that promotes C-S bond cleavage. Conversely, with respect to the methyl radical mechanism, the results do not rule out a requirement for HSCoB in hydrogen atom abstraction or in promoting a conformational change that might alter the reaction pathway and/or the regioselectivity of the attack of Ni^{I} on methyl-SCoM.

HSCoM is firmly held in the active site of MCR by interactions of the thiol group with nickel, one of the sulfonate oxygens with a backbone nitrogen in the α subunit, and another sulfonate oxygen with Arg-120 of the γ subunit (Fig. 10). The interactions of the sulfonate oxygens greatly influence the type of substrate that can react with MCR. When the structures of the various sulfonate and carboxylate analogs shown in Table 1 are compared, it appears that generation of the MCR_{PS} signal requires a good leaving group adjacent to an electrophilic carbon atom that is four bonds (~ 4.8 Å) from the negatively charged oxygen of a carboxylate or sulfonate. When this distance is increased to ~ 6 Å with BBS, the second order rate constant for reaction of MCR_{red1} with the bromoalkanesulfonate decreases by 70-fold. Interestingly, the electrophilic carbon in BPS is in the same position as the thioether sulfur of methyl-SCoM and the bromine group of BPS is located at approximately the same position as the methyl group of methyl-SCoM. These results indicate that, for the natural substrate, steric considerations would favor attack of Ni(I) at the sulfur of methyl-SCoM. However, as mentioned above, it is possible that binding of HSCoB could alter the stereoselectivity of the active site.

By strict analogy with the BPS reaction and as shown in Fig. 11B, in which attack of Ni(I) on C-3 of BPS followed by elimination of the bromide would generate the MCR_{PS} state, one might expect Ni(I) to react with the thioether sulfur of methyl-SCoM to generate a Ni(III)-thiolate and eliminate a methyl anion. However, the poor leaving group properties of a methyl group as discussed above would prevent such a reaction. On the other hand, the attack of Ni(I) on the thioether sulfur of methyl-SCoM to form a Ni(III)-thiolate and release a methyl radical, as described in Fig. 11C, would retain the steric constraints of the reaction, based on the substrate profile described in the legend to Fig. 1. This step, leading to the formation of a relatively strong Ni(III)–thiolate bond and release of a methyl radical, was proposed to be feasible, with a barrier of ~ 17 – 20 kcal/mol⁸ (instead of ~ 45 kcal/mol for generation of the methyl-Ni) (27). Hydrogen atom abstraction from HSCoB by the methyl radical to form methane was predicted to have a very small barrier of ~ 1 kcal/mol (27).

As shown in Fig. 11C, the reaction of MCR_{PS} with a thiolate to form the thioether and regenerate MCR_{red1} is similar to the proposed reaction of the CoBS radical with the Ni(III)-thiolate to generate the disulfide anion radical and a Ni(II) form of MCR (Fig. 11C). Electron transfer from the disulfide anion radical to Ni(II) would form the disulfide and Ni(I)- MCR_{red1} . Interestingly, in methane formation, cleavage of the C–S bond of methyl-SCoM appears to be rate-limiting, whereas in the BPS reaction, the first step (elimination of bromide) is rapid, and regeneration of MCR_{red1} is rate-limiting.

In conclusion, the results described here are relevant to the initial step in methane formation and to the final step in anaerobic methane oxidation. Further studies involving analogs of methyl-SCoM and HSCoB are under way to uncover details of

the MCR catalytic mechanism and to discriminate between the two proposed mechanisms for this unique nickel enzyme.

Acknowledgment—We thank Dr. Mishtu Dey for helpful discussions.

REFERENCES

1. Thauer, R. K. (1998) *Microbiology* **144**, 2377–2406
2. DiMarco, A. A., Bobik, T. A., and Wolfe, R. S. (1990) *Annu. Rev. Biochem.* **59**, 355–394
3. Ellermann, J., Kobelt, A., Pfaltz, A., and Thauer, R. K. (1987) *FEBS Lett.* **220**, 358–362
4. Diekert, G., Klee, B., and Thauer, R. K. (1980) *Arch. Microbiol.* **124**, 103–106
5. Diekert, G., Jaenchen, R., and Thauer, R. K. (1980) *FEBS Lett.* **119**, 118–120
6. Whitman, W. B., and Wolfe, R. S. (1980) *Biochem. Biophys. Res. Commun.* **92**, 1196–1201
7. Ermler, U., Grabarse, W., Shima, S., Goubeaud, M., and Thauer, R. K. (1997) *Science* **278**, 1457–1462
8. Albracht, S. P. J., Ankel-Fuchs, D., Böcher, R., Ellermann, J., Moll, J., van der Zwann, J. W., and Thauer, R. K. (1988) *Biochim. Biophys. Acta* **941**, 86–102
9. Rospert, S., Böcher, R., Albracht, S. P. J., and Thauer, R. K. (1991) *FEBS Lett.* **291**, 371–375
10. Goubeaud, M., Schreiner, G., and Thauer, R. K. (1997) *Eur. J. Biochem.* **243**, 110–114
11. Becker, D. F., and Ragsdale, S. W. (1998) *Biochemistry* **37**, 2639–2647
12. Grabarse, W. G., Mahler, F., Shima, S., Thauer, R. K., and Ermler, U. (2000) *J. Mol. Biol.* **303**, 329–344
13. Grabarse, W. G., Mahler, F., Duin, E. C., Goubeaud, M., Shima, S., Thauer, R. K., Lamzin, V., and Ermler, U. (2001) *J. Mol. Biol.* **309**, 315–330
14. Duin, E. C., Cosper, N. J., Mahler, F., Thauer, R. K., and Scott, R. A. (2003) *J. Biol. Inorg. Chem.* **8**, 141–148
15. Craft, J. L., Horng, Y.-C., Ragsdale, S. W., and Brunold, T. C. (2004) *J. Am. Chem. Soc.* **126**, 4068–4069
16. Craft, J. L., Horng, Y. C., Ragsdale, S. W., and Brunold, T. C. (2004) *J. Biol. Inorg. Chem.* **9**, 77–89
17. Harmer, J., Finazzo, C., Piskorski, R., Bauer, C., Jaun, B., Duin, E. C., Goenrich, M., Thauer, R. K., Van Doorslaer, S., and Schweiger, A. (2005) *J. Am. Chem. Soc.* **127**, 17744–17755
18. Tang, Q., Carrington, P. E., Horng, Y.-C., Maroney, M. J., Ragsdale, S. W., and Bocian, D. F. (2002) *J. Am. Chem. Soc.* **124**, 13242–13256
19. Singh, K., Horng, Y. C., and Ragsdale, S. W. (2003) *J. Am. Chem. Soc.* **125**, 2436–2443
20. Berkessel, A. (1991) *Biorganic Chem.* **19**, 101–115
21. Jaun, B. (1990) *Helv. Chem. Acta* **73**, 2209–2216
22. Signor, L., Knappe, C., Hug, R., Schweizer, B., Pfaltz, A., and Jaun, B. (2000) *Chemistry* **6**, 3508–3516
23. Horng, Y.-C., Becker, D. F., and Ragsdale, S. W. (2001) *Biochemistry* **40**, 12875–12885
24. Lin, S.-K., and Jaun, B. (1992) *Helv. Chem. Acta* **75**, 1478–1490
25. Lin, S.-K., and Jaun, B. (1991) *Helv. Chem. Acta* **74**, 1725–1738
26. Lahiri, G. K., and Stolzenberg, A. M. (1993) *Inorg. Chem.* **32**, 4409–4413
27. Pelmentschikov, V., Blomberg, M. R. A., Siegbahn, P. E. M., and Crabtree, R. H. (2002) *J. Am. Chem. Soc.* **124**, 4039–4049
28. Rospert, S., Voges, M., Berkessel, A., Albracht, S. P. J., and Thauer, R. K. (1992) *Eur. J. Biochem.* **210**, 101–107
29. Goenrich, M., Mahler, F., Duin, E. C., Bauer, C., Jaun, B., and Thauer, R. K. (2004) *J. Biol. Inorg. Chem.* **9**, 691–705
30. Gunsalus, R. P., Romesser, J. A., and Wolfe, R. S. (1978) *Biochemistry* **17**, 2374–2377
31. Bobik, T. A., and Wolfe, R. S. (1988) *Proc. Natl. Acad. Sci. U. S. A.* **85**, 60–63
32. Noll, K. M., Donnelly, M. I., and Wolfe, R. S. (1987) *J. Biol. Chem.* **262**, 513–515
33. Ellermann, J., Hedderich, R., Böcher, R., and Thauer, R. K. (1988) *Eur.*

⁸ The DFT calculations suggest that release of the methyl radical has a barrier of 19.5 kcal/mol, and formation of the bond between Ni(II) and the thiol sulfur of CoM has a barrier of 38.6 kcal/mol, yielding a net barrier for this step in the proposed reaction cycle of ~ 20 kcal/mol.

- J. Biochem.* **172**, 669–677
34. Riddles, P. W., Blakeley, R. L., and Zerner, B. (1979) *Anal. Biochem.* **94**, 75–81
35. Zehnder, A. J. B., and Wuhrmann, K. (1976) *Science* **194**, 1165–1166
36. Schönheit, P., Moll, J., and Thauer, R. K. (1980) *Arch. Microbiol.* **127**, 59–65
37. Mählert, F., Bauer, C., Jaun, B., Thauer, R. K., and Duin, E. C. (2002) *J. Biol. Inorg. Chem.* **7**, 500–513
38. Bradford, M. M. (1976) *Anal. Biochem.* **72**, 248–254
39. Pfaltz, A., Juan, B., Fassler, A., Eschenmoser, A., Jaenchen, R., Gilles, H. H., Diekert, G., and Thauer, R. K. (1982) *Helv. Chim. Acta* **65**, 828–865
40. Di Tusa, M. R., and Schilt, A. A. (1985) *J. Chem. Ed.* **62**, 541–542
41. Ellermann, J., Rospert, S., Thauer, R. K., Bokranz, M., Klein, A., Voges, M., and Berkessel, A. (1989) *Eur. J. Biochem.* **184**, 63–68
42. Rospert, S., Linder, D., Ellermann, J., and Thauer, R. K. (1990) *Eur. J. Biochem.* **194**, 871–877
43. Good, N. E., Winget, G. D., Winter, W., Connolly, T. N., Izawa, S., and Singh, R. M. (1966) *Biochemistry* **5**, 467–477
44. Goenrich, M., Duin, E. C., Mählert, F., and Thauer, R. K. (2005) *J. Biol. Inorg. Chem.* **10**, 333–342
45. Holliger, C., Pierik, A. J., Reijerse, E. J., and Hagen, W. R. (1993) *J. Am. Chem. Soc.* **115**, 5651–5656
46. Banerjee, R., and Ragsdale, S. W. (2003) *Annu. Rev. Biochem.* **72**, 209–247
47. Brenner, M. C., Zhang, H., and Scott, R. A. (1993) *J. Biol. Chem.* **268**, 18491–18495
48. Hinderberger, D., Piskorski, R. P., Goenrich, M., Thauer, R. K., Schweiger, A., Harmer, J., and Jaun, B. (2006) *Angew. Chem. Int. Ed. Engl.* **45**, 3602–3607
49. Wondimagegn, T., and Ghosh, A. (2001) *J. Am. Chem. Soc.* **123**, 1543–1544
50. Pel'menschikov, V., and Siegbahn, P. E. (2003) *J. Biol. Inorg. Chem.* **8**, 653–662

Spectroscopic and Kinetic Studies of the Reaction of Bromopropanesulfonate with Methyl-coenzyme M Reductase

Ryan C. Kunz, Yih-Chern Horng and Stephen W. Ragsdale

J. Biol. Chem. 2006, 281:34663-34676.

doi: 10.1074/jbc.M606715200 originally published online September 11, 2006

Access the most updated version of this article at doi: [10.1074/jbc.M606715200](https://doi.org/10.1074/jbc.M606715200)

Alerts:

- [When this article is cited](#)
- [When a correction for this article is posted](#)

[Click here](#) to choose from all of JBC's e-mail alerts

Supplemental material:

<http://www.jbc.org/content/suppl/2006/09/12/M606715200.DC1>

This article cites 50 references, 5 of which can be accessed free at

<http://www.jbc.org/content/281/45/34663.full.html#ref-list-1>